Journal of Biomolecular NMR, 7 (1996) 142–152
ESCOM

J-Bio NMR 330

Heteronuclear relayed E.COSY applied to the determination of accurate $^3J(H^N,C')$ and $^3J(H^\beta,C')$ coupling constants in *Desulfovibrio vulgaris* flavodoxin

Jürgen M. Schmidt, Frank Löhr and Heinz Rüterjans*

Institut für Biophysikalische Chemie, Johann Wolfgang Goethe Universität Frankfurt am Main, Biozentrum, Marie Curie Strasse 9, D-60439 Frankfurt am Main, Germany

Received 27 October 1995
Accepted 2 January 1996

Keywords: Multiplet simulation; Least-squares optimization; Spectrum fitting; Long-range couplings

Summary

A simple constant-time 3D heteronuclear NMR pulse sequence has been developed to quantitatively determine the heteronuclear three-bond couplings $^3J(H^N,C')$ and $^3J(H^\beta,C')$ in uniformly ^{13}C-enriched proteins. The protocols for measuring accurate coupling constants are based on $^1H,^{13}C$-heteronuclear relayed E.COSY [Schmidt, J.M., Ernst, R.R., Aimoto, S. and Kainosho, M. (1995) *J. Biomol. NMR*, **6**, 95–105] in combination with numerical least-squares spectrum evaluation. Accurate coupling constants are extracted from 2D spectrum projections using 2D multiplet simulation. Confidence intervals for the obtained three-bond coupling constants are calculated from F-statistics. The three-bond couplings are relevant to the determination of ϕ and χ_1 dihedral-angle conformations in the amino acid backbone and side chain. The methods are demonstrated on the recombinant $^{13}C,^{15}N$-doubly enriched 147-amino acid protein *Desulfovibrio vulgaris* flavodoxin with bound flavin mononucleotide in its oxidized form. In total, 109 $^3J(H^N,C')$ and 100 $^3J(H^\beta,C')$ coupling constants are obtained from a single spectrum.

Introduction

Structure determination of biological macromolecules in solution by NMR methods (Wüthrich, 1986) increasingly relies on the measurement of nuclear spin–spin couplings (Biamonti et al., 1994; Case et al., 1994; Eberstadt et al., 1995). The magnitude of the observed coupling constants relates to the dihedral angle subtended by those three successive covalent bonds that connect the coupling nuclei (Karplus, 1959,1963). Recently, $^1H,^{13}C$-heteronuclear long-range couplings have been determined by the heteronuclear relayed E.COSY technique, as demonstrated on a uniformly ^{13}C-labeled peptide sample (Schmidt et al., 1995). From a single C^α,H^N multiplet, the coupling constants $^3J(H^N,C')$ and $^3J(H^N,C^\beta)$ were obtained, which are relevant to the conformation of backbone ϕ torsions in polypeptides. From the respective C^α,H^β and C^β,H^α multiplets in the same 2D spectrum, $^3J(H^\beta,C')$ and $^3J(H^\alpha,C^\gamma)$ were obtained, which define the side-chain dihedral angle χ_1. The heteronuclear relayed E.COSY concept outlined by Schmidt et al. (1995) motivated the design of a modified pulse scheme that can be applied in cases where line widths are large, in particular for studying coupling constants in proteins. Here we report on the determination of $^3J(H^N,C')$ and $^3J(H^\beta,C')$ coupling constants in *Desulfovibrio vulgaris* flavodoxin (Mayhew and Ludwig, 1975; Mayhew and Tollin, 1992) in order to support the accurate determination of its torsion-angle conformations.

Desulfovibrio vulgaris flavodoxin is a member of a group of small microbial electron-transfer proteins containing noncovalently bound flavin mononucleotide (FMN) as the redox-active group. The protein chain consists of 147 amino acid residues (the recombinant form aligns with residues 2 through 148 of the native sequence) with a molecular mass of 16.3 kDa (Dubour-

*To whom correspondence should be addressed.

Abbreviations: ANOVA, analysis of variances; COSY, correlated spectroscopy; E.COSY, exclusive correlation spectroscopy; FMN, flavin mononucleotide; HMQC, heteronuclear multiple-quantum coherence; HSQC, heteronuclear single-quantum coherence.

dieu and Fox, 1977). The redox properties of *D. vulgaris* flavodoxin have been reviewed (Ghisla and Massey, 1989). Flavodoxins are known to interact with other redox proteins, although their role in electron transfer mechanisms is not yet well understood.

A number of flavodoxins have been studied by both crystallographic and NMR methods. The crystal structures of *D. vulgaris* flavodoxin in three different oxidation states, maintained at liquid-nitrogen temperature, have been determined with 0.2 nm resolution (Watt et al., 1991). The solution structure was refined on the basis of 1350 interproton distances, obtained from homonuclear and $^{1}H,^{15}N$-heteronuclear NMR spectra (Knauf et al., 1993,1996).

Theory

Heteronuclear relayed E.COSY (Schmidt et al., 1995) relies on the presence of a cyclic four-spin coupling topology ($-I_2-I_1-S_1-S_2-$) where I and S denote proton and – in the present case – carbon spins, respectively. The interaction between two active spins S_1 and I_2, mediated through simultaneous couplings to the auxiliary (relay) spin I_1, gives rise to a multiplet appearing at the coordinates $(\omega_{S_1},\omega_{I_2})$ in a 2D spectrum. S_2 is identified with the passive spin whose interaction with I_2 , i.e. the coupling constant $J_{I_2S_2}$, is the desired structure parameter. The basic response calculation for the heteronuclear two-dimensional pulse experiment has been presented by Schmidt et al. (1995). Here the modifications and generalizations brought about by the proposed 3D experiment are discussed.

Equilibrium proton magnetization, $\sigma_0 = I_{1z}$, is subject to an initial nonselective $\{\pi/2\}_{I_x}$ proton excitation pulse, as indicated in Fig. 1. Following duration τ, which is adjusted to $(2J_{I_1S_1})^{-1}$, the first selective $\{\pi/2\}_{S_{1x}}$ pulse converts heteronuclear I_1S_1 antiphase magnetization to yield the two essential multiple-quantum terms in the density operator evolution according to:

$$\sigma_1 = -2I_{1x}S_{1y}\cos(\pi J_{I_1I_2}\tau) - 4I_{1y}S_{1y}I_{2z}\sin(\pi J_{I_1I_2}\tau) \quad (1)$$

In the further course of the experiment, coherence propagates from the present I_1S_1 multiple-quantum coherence to the target spin I_2, whose magnetization is finally detected. Similar to the homonuclear relayed E.COSY experiment (Schmidt et al., 1994), coherence transfer is mediated through two competitive pathways, i.e. via the coupling $J_{I_1I_2}$ and, to a lesser extent, via the usually smaller coupling $J_{S_1I_2}$. The two possible paths will be associated with *relayed* ($S_1 \rightarrow I_1 \rightarrow I_2$) and *direct* ($S_1 \rightarrow I_2$) interaction, respectively.

To elucidate the 3D multiplet composition, the initial analysis will be restricted to the $-I_2-I_1-S_1-$ three-coupling/three-spin subsystem, the chemical shifts of which potentially give rise to three spectrum dimensions. Preferentially, the dimensions of a 2D subspectrum are spanned by the chemical shifts associated with S_1 and I_2, while I_1 chemical shifts usually are of minor preference and are rather used for separating congested spectrum regions into a third dimension. In the very first ($t_1 = 0, t_2 = 0, t_3$) increment, chemical-shift precession of both S and I spins is refocused due to the pair of π pulses centered within the constant period T. However, in subsequent 3D increments, both S and I chemical shifts evolve during t_1 and t_2, respectively. A number of J couplings evolve,

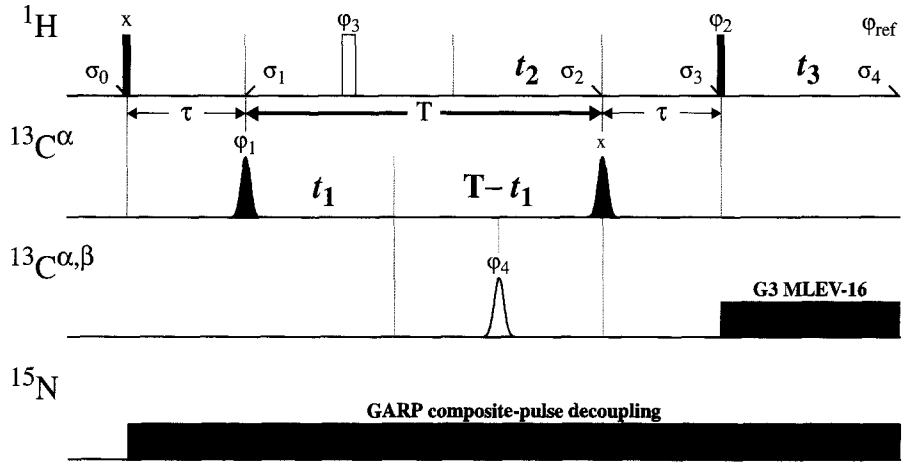

Fig. 1. Pulse sequence of the 3D constant-time heteronuclear relayed E.COSY experiment for the determination of the heteronuclear three-bond couplings $^{3}J(H^{N},C')$ and $^{3}J(H^{\beta},C')$ as applied to *Desulfovibrio vulgaris* flavodoxin. Filled and open symbols represent $\pi/2$ and π pulses, respectively. Aliphatic carbon spins are selectively excited, as indicated by Gaussian-shaped symbols, to prevent state mixing of passive carbonyl carbon spins. Continuous GARP decoupling is applied to ^{15}N nuclei, to avoid unwanted multiplet splittings. The basic phase cycle is $\varphi_1 = x,-x,x,-x$; $\varphi_2 = y,y,-y,-y$; $\varphi_{ref} = x,-x,x,-x$. The two-step phase cycle (φ_2) imposed on the final proton mixing pulse suppresses higher order multiple-quantum contributions and may be extended appropriately if more complicated spin topologies are considered. After four scans, the ^{1}H refocussing pulse phase was changed according to $\varphi_3 = 4(x),4(y)$ with concomitant inversion of the receiver phase. After eight scans, the 180° G3 refocussing pulse phase φ_4 was inverted without altering the receiver phase.

leading to the relevant spin operators at the end of the interval T given by:

$$\begin{aligned}\sigma_2 = 2I_{1x}S_{1y}[&\cos(\pi J_{I_1I_2}(T+\tau))\cos(\pi J_{S_1I_2}(T-t_1-t_2))\\ &\times\cos(\omega_{I_1}t_2)\cos(\omega_{S_1}t_1)\\ &+\sin(\pi J_{I_1I_2}(T+\tau))\sin(\pi J_{S_1I_2}(T-t_1-t_2))\\ &\times\sin(\omega_{I_1}t_2)\sin(\omega_{S_1}t_1)]\\ +4I_{1y}S_{1y}I_{2z}[&\cos(\pi J_{I_1I_2}(T+\tau))\sin(\pi J_{S_1I_2}(T-t_1-t_2))\\ &\times\sin(\omega_{I_1}t_2)\sin(\omega_{S_1}t_1)\\ &-\sin(\pi J_{I_1I_2}(T+\tau))\cos(\pi J_{S_1I_2}(T-t_1-t_2))\\ &\times\cos(\omega_{I_1}t_2)\cos(\omega_{S_1}t_1)]\end{aligned} \quad (2)$$

where the effect of the refocusing π pulses has been incorporated. The second selective $\{\pi/2\}_{S_{1x}}$ pulse restores heteronuclear I_1S_1 antiphase magnetization, which refocuses under the coupling $J_{I_1S_1}$ during the second period τ to yield the relevant terms

$$\begin{aligned}\sigma_3 = 2I_{1x}I_{2z}[&\cos(\pi J_{I_1I_2}(T+2\tau))\sin(\pi J_{S_1I_2}(T-t_1-t_2))\\ &\times\sin(\omega_{I_1}t_2)\sin(\omega_{S_1}t_1)\\ &-\sin(\pi J_{I_1I_2}(T+2\tau))\cos(\pi J_{S_1I_2}(T-t_1-t_2))\\ &\times\cos(\omega_{I_1}t_2)\cos(\omega_{S_1}t_1)]\end{aligned} \quad (3)$$

The final $\{\pi/2\}_{I_y}$ proton mixing pulse transfers polarization to the I_2 spin, which evolves into observable magnetization (pure absorption component) according to:

$$\begin{aligned}\sigma_4 = I_{2y}&\sin(\pi J_{I_1I_2}t_3)\sin(\omega_{I_2}t_3)\\ \times[&\cos(\pi J_{I_1I_2}(T+2\tau))\sin(\pi J_{S_1I_2}(T-t_1-t_2))\\ &\times\sin(\omega_{I_1}t_2)\sin(\omega_{S_1}t_1)\\ &-\sin(\pi J_{I_1I_2}(T+2\tau))\cos(\pi J_{S_1I_2}(T-t_1-t_2))\\ &\times\cos(\omega_{I_1}t_2)\cos(\omega_{S_1}t_1)]\end{aligned} \quad (4)$$

These are the two contributions giving rise to a composite basic correlation multiplet at coordinates $(\omega_{S_1},\omega_{I_1},\omega_{I_2})$ in a 3D spectrum. The first product term in the brackets in Eq. 4 arises from the direct $S_1 \rightarrow I_2$ interaction, while the second product term is due to the $S_1 \rightarrow I_1 \rightarrow I_2$ relayed coherence transfer pathway.

Now, the passive spin S_2 will be reintroduced, assuming nonvanishing couplings to the three active spins S_1, I_1, and I_2. These couplings give rise to E.COSY-type multiplet splittings in each spectrum dimension, as the S_2 spin states are conserved due to selective excitation techniques. The effect is described by:

$$\begin{aligned}\sigma_4' = \sigma_4 \times &\{\cos(\pi J_{S_1S_2}t_1) - 2S_{2z}\sin(\pi J_{S_1S_2}t_1)\}\\ \times &\{\cos(\pi J_{I_1S_2}t_2) - 2S_{2z}\sin(\pi J_{I_1S_2}t_2)\}\\ \times &\{\cos(\pi J_{I_2S_2}t_3) - 2S_{2z}\sin(\pi J_{I_2S_2}t_3)\}\end{aligned} \quad (5)$$

Utilizing the polarization operators $S_2^\alpha = 1/2 + S_{2z}$ and $S_2^\beta = 1/2 - S_{2z}$ as well as the composite frequencies $\Sigma_1 = \omega_{S_1} + \pi J_{S_1S_2}$, $\Delta_1 = \omega_{S_1} - \pi J_{S_1S_2}$, $\Sigma_2 = \omega_{I_1} + \pi J_{I_1S_2}$, $\Delta_2 = \omega_{I_1} - \pi J_{I_1S_2}$, $\Sigma_3 = \omega_{I_2} + \pi J_{I_2S_2}$ and $\Delta_3 = \omega_{I_2} - \pi J_{I_2S_2}$, the chemical-shift terms in Eq. 4 are replaced correspondingly and Eq. 5 is recast to:

$$\begin{aligned}\sigma_4' = I_{2y}&\sin(\pi J_{I_1I_2}t_3)\{S_2^\alpha\cos(\Sigma_3t_3) + S_2^\beta\cos(\Delta_3t_3)\}\\ \times[&\cos(\pi J_{I_1I_2}(T+2\tau))\sin(\pi J_{S_1I_2}(T-t_1-t_2))\\ &\times\{S_2^\alpha\sin(\Sigma_1t_1) + S_2^\beta\sin(\Delta_1t_1)\}\\ &\times\{S_2^\alpha\sin(\Sigma_2t_2) + S_2^\beta\sin(\Delta_2t_2)\}\\ &-\sin(\pi J_{I_1I_2}(T+2\tau))\cos(\pi J_{S_1I_2}(T-t_1-t_2))\\ &\times\{S_2^\alpha\cos(\Sigma_1t_1) + S_2^\beta\cos(\Delta_1t_1)\}\\ &\times\{S_2^\alpha\cos(\Sigma_2t_2) + S_2^\beta\cos(\Delta_2t_2)\}]\end{aligned} \quad (6)$$

For both relayed and direct contributions, the observable terms $I_{2y}S_2^\alpha$, $I_{2y}S_2^\beta$ and, in quadrature-detection mode, $I_{2x}S_2^\alpha$, $I_{2x}S_2^\beta$, lead to two multiplet components located at positions $(\Sigma_1,\Sigma_2,\Sigma_3)$ and $(\Delta_1,\Delta_2,\Delta_3)$ in a 3D spectrum. This is the expected typical E.COSY multiplet pattern (Griesinger et al., 1986) extending over all three dimensions, which allows the desired coupling constant $J_{I_2S_2}$ to be determined from the displacement

$$J_{I_2S_2} = (\Sigma_3 - \Delta_3)/2\pi \quad (7)$$

The intensity ratio of direct to relayed multiplet contributions is determined by an amplitude factor $\{-\tan(\pi J_{S_1I_2}T) / \tan(\pi J_{I_1I_2}(T+2\tau))\}$, which depends mainly on the relative magnitude of both active couplings $J_{I_1I_2}$ and $J_{S_1I_2}$ and less on the fixed periods T and τ. Note that in Eqs. 4 and 6, the chemical-shift operators of relayed and direct multiplet contributions are 90° out of phase, i.e. they represent pure absorption and pure dispersion components, respectively, in both indirectly sampled dimensions ω_1 and ω_2. However, both multiplet contributions exhibit identical phase and splitting properties in the acquisition dimension ω_3, where the most prominent effect is an antiphase doublet with respect to the active homonuclear coupling $J_{I_1I_2}$. The splittings along ω_1 and ω_2 due to

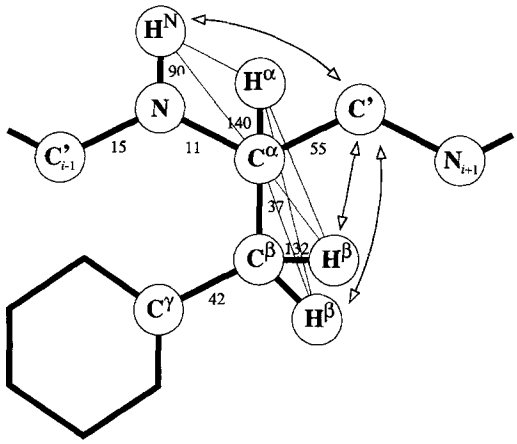

Fig. 2. Schematic representation of the amino acid spin-coupling topology in ^{13}C-enriched proteins, exploited for the determination of three-bond coupling constants by heteronuclear relayed E.COSY. Numbers indicate magnitudes of one-bond J-couplings (in Hz). Active couplings, which are essential for the coherence transfer, are indicated by light lines. Arrows indicate the heteronuclear three-bond couplings examined in the context of the present investigation. The large passive $^1J(C^\alpha,C')$ coupling (~ 55 Hz) is used for separating the two halves in E.COSY-type C^α,H^N and C^α,H^β multiplets.

TABLE 1
FIT PARAMETERS USED IN MULTIPLET MODELLING

Parameter type	Dimension	Association	
		C^{α},H^{N} multiplet	C^{α},H^{β} multiplet
Global scale		A	A
Zero-order phase[a]	F1	φ	φ
Apparent line width	F3	$R(H^{N})$	$R(H^{\beta})$
Position[b]	F1	$\Omega(C^{\alpha})$	$\Omega(C^{\alpha})$
Position	F3	$\Omega(H^{N})$	$\Omega(H^{\beta})$
Direct-transfer coupling	F1	$J(C^{\alpha},H^{N})$	$J(C^{\alpha},H^{\beta})$
Relayed-transfer coupling	F3	$J(H^{N},H^{\alpha})$	$J(H^{\beta},H^{\alpha})$
E.COSY splitting	F1	$J(C^{\alpha},C_{i}')$	$J(C^{\alpha},C_{i}')$
E.COSY splitting	F3	$J(H^{N},C_{i}')$	$J(H^{\beta},C_{i}')$
In-phase splitting[c]	F1	$J(H^{l},C^{\alpha})$, $J(H^{\alpha},C^{m})$	$J(H^{l},C^{\alpha})$, $J(H^{\alpha},C^{m})$
In-phase splitting	F3	$J(H^{N},C_{i-1}')$	$J(H^{\beta},C^{n})$

[a] Based on Eq. 8, the real and imaginary components of the complex factor $\exp(i2\pi\varphi)$ are used to fine-adjust the mixing ratio of direct to relayed multiplet contributions, to account for residual distortions due to 2D projection.

[b] Positional parameters refer to the center coordinates of the selected multiplet submatrix.

[c] The numerically very similar modulations involving couplings to spins H^{α} and C^{α} do not allow for significant separation of the various splitting effects given in Eq. 9. Thus, for the C^{α},H^{N} multiplet, the indices denote combined effects from remote coupled nuclei $H^{l}=H^{\beta},H^{\gamma}$; $C^{m}=C^{\beta},C^{\gamma}$ in most amino acids. For the C^{α},H^{β} multiplet, $H^{l}=H^{N},H^{\beta},H^{\gamma}$; $C^{m}=C^{\beta},C^{\gamma}$ in aliphatic side chains, while $C^{n}=C^{\gamma}$ in aromatic side chains and Asx residues, and $C^{n}=C^{\delta}$ in aromatic side chains and Glx residues.

homo- and heteronuclear couplings, indicated in Eqs. 4 and 6, are rationalized using the following identities:

$$\begin{aligned}\cos(\pi J(T\pm t)) &= \cos(\pi JT)\cos(\pi Jt) \mp \sin(\pi JT)\sin(\pi Jt)\\ \sin(\pi J(T\pm t)) &= \sin(\pi JT)\cos(\pi Jt) \pm \cos(\pi JT)\sin(\pi Jt)\end{aligned} \quad (8)$$

where T is the constant-time period and t is one of the time variables t_1 or t_2. In essence, the modulation due to the active heteronuclear coupling $J_{S_1I_2}$ is expressed as a superposition of in-phase and antiphase J-splitting patterns, controlled by the mixing ratio $\tan(\pi J_{S_1I_2}T)$. Usually, $J_{S_1I_2} \ll T^{-1}$ so that the coefficient $\sin(\pi J_{S_1I_2}T)$ in Eq. 8 is expected to be small.

In ^{13}C-labeled amino acids, a variety of heteronuclear three-bond couplings is encountered. A judicious choice of the basic four-spin coupling topology allows the determination of particularly important three-bond coupling constants in polypeptides by heteronuclear relayed E.COSY, as indicated in Fig. 2. The coupling constant $^3J(H^N,C')$ is accessible if I_2, I_1, S_1 and S_2 are identified with H^N, H^{α}, C^{α} and C', respectively, where the large $^1J(C^{\alpha},C')$ coupling is exploited for the separation of the two E.COSY multiplet halves. Similarly, $^3J(H^{\beta},C')$ coupling constants can be determined based on the four-spin coupling topology comprising H^{β}, H^{α}, C^{α} and C'. The multiplet for evaluating the $^3J(H^N,C')$ coupling constant is then located at $(\Omega_{C^{\alpha}}, \Omega_{H^{\alpha}}, \Omega_{H^N})$ in the 3D spectrum, while that for evaluating the $^3J(H^{\beta},C')$ coupling constant is found at $(\Omega_{C^{\alpha}}, \Omega_{H^{\alpha}}, \Omega_{H^{\beta}})$.

Although overlap is sufficiently reduced by a few t_2 increments spreading H^{α} chemical shifts into the ω_2 dimension, heteronuclear couplings like $^2J(H^{\alpha},C')$ are not resolved in the ω_2 dimension, as they are usually small compared to the digital resolution and the line width. This allows two-dimensional (ω_1,ω_3) projections to be computed for a quantitative multiplet analysis. Ideally, the pure dispersion components along ω_2 due to direct coherence transfer cancel by summing over neighbouring spectrum planes. Provided that $\tau = (2J_{H^{\alpha}C^{\alpha}})^{-1}$ and $T = (J_{C^{\alpha}C^{\beta}})^{-1}$, the dependence of the observable magnetization on the various chemical-shift and coupling terms for the relayed contribution to the three-dimensional $C^{\alpha},H^{\alpha},H^N$ multiplet is summarized as follows:

$$\begin{aligned}\sigma_{obs} = I_{y,H^N} &\{ S^{\alpha}_{C'}\cos(\Sigma_3 t_3) + S^{\beta}_{C'}\cos(\Delta_3 t_3)\}\\ &\times \sin(\pi J_{H^NH^{\alpha}} t_3)\prod_k \cos(\pi J_{H^{\alpha}H^k}(T+2\tau))\\ &\times \prod_l \cos(\pi J_{H^lC^{\alpha}}(T-t_2-t_1))\\ &\times \prod_m \cos(\pi J_{H^{\alpha}C^m}(T+2\tau-t_2-t_1))\prod_n \cos(\pi J_{H^NC^n}t_3)\\ &\times [\cos(\pi J_{H^NH^{\alpha}}(T+2\tau))\sin(\pi J_{H^NC^{\alpha}}(T-t_1-t_2))\\ &\quad\times \{ S^{\alpha}_{C'}\sin(\Sigma_1 t_1) + S^{\beta}_{C'}\sin(\Delta_1 t_1)\}\\ &\quad\times \{ S^{\alpha}_{C'}\sin(\Sigma_2 t_2) + S^{\beta}_{C'}\sin(\Delta_2 t_2)\}\\ &\quad - \sin(\pi J_{H^NH^{\alpha}}(T+2\tau))\cos(\pi J_{H^NC^{\alpha}}(T-t_1-t_2))\\ &\quad\times \{ S^{\alpha}_{C'}\cos(\Sigma_1 t_1) + S^{\beta}_{C'}\cos(\Delta_1 t_1)\}\\ &\quad\times \{ S^{\alpha}_{C'}\cos(\Sigma_2 t_2) + S^{\beta}_{C'}\cos(\Delta_2 t_2)\}]\end{aligned} \quad (9)$$

where k, l, m, and n denote remote proton or carbon spins as found in amino acid spin topologies, excluding the basic spins H^N, H^{α}, C^{α} and C', respectively. The sum and difference symbols then translate to $\Sigma_1 = \Omega_{C^{\alpha}} + \pi J_{C^{\alpha}C'}$ and $\Delta_1 = \Omega_{C^{\alpha}} - \pi J_{C^{\alpha}C'}$, $\Sigma_2 = \Omega_{H^{\alpha}} + \pi J_{H^{\alpha}C'}$, $\Delta_2 = \Omega_{H^{\alpha}} - \pi J_{H^{\alpha}C'}$, $\Sigma_3 = \Omega_{H^N} + \pi J_{H^NC'}$, and $\Delta_3 = \Omega_{H^N} - \pi J_{H^NC'}$. In full analogy, Eq. 9 also applies to the $C^{\alpha},H^{\alpha},H^{\beta}$ multiplet if H^N designations are appropriately replaced by H^{β}.

Materials and Methods

Sample preparation

Recombinant $^{13}C,^{15}N$-doubly enriched *Desulfovibrio vulgaris* flavodoxin was grown in *E. coli* according to the protocols of Curley et al. (1991). The NMR sample was prepared from 18 mg of the lyophilized protein to yield a concentration of 2.2 mM in 500 µl potassium phosphate buffer, pH 7, containing 5% D_2O and 0.02% NaN_3. ^1H chemical shifts refer to external 3-trimethylsilyl-2,2',3,3'-d_4-propionate sodium salt (TSP). The proton and nitrogen resonance assignments in *D. vulgaris* flavodoxin have been reported previously (Knauf et al., 1993). Carbon resonance assignments have been carried out and will be published elsewhere.

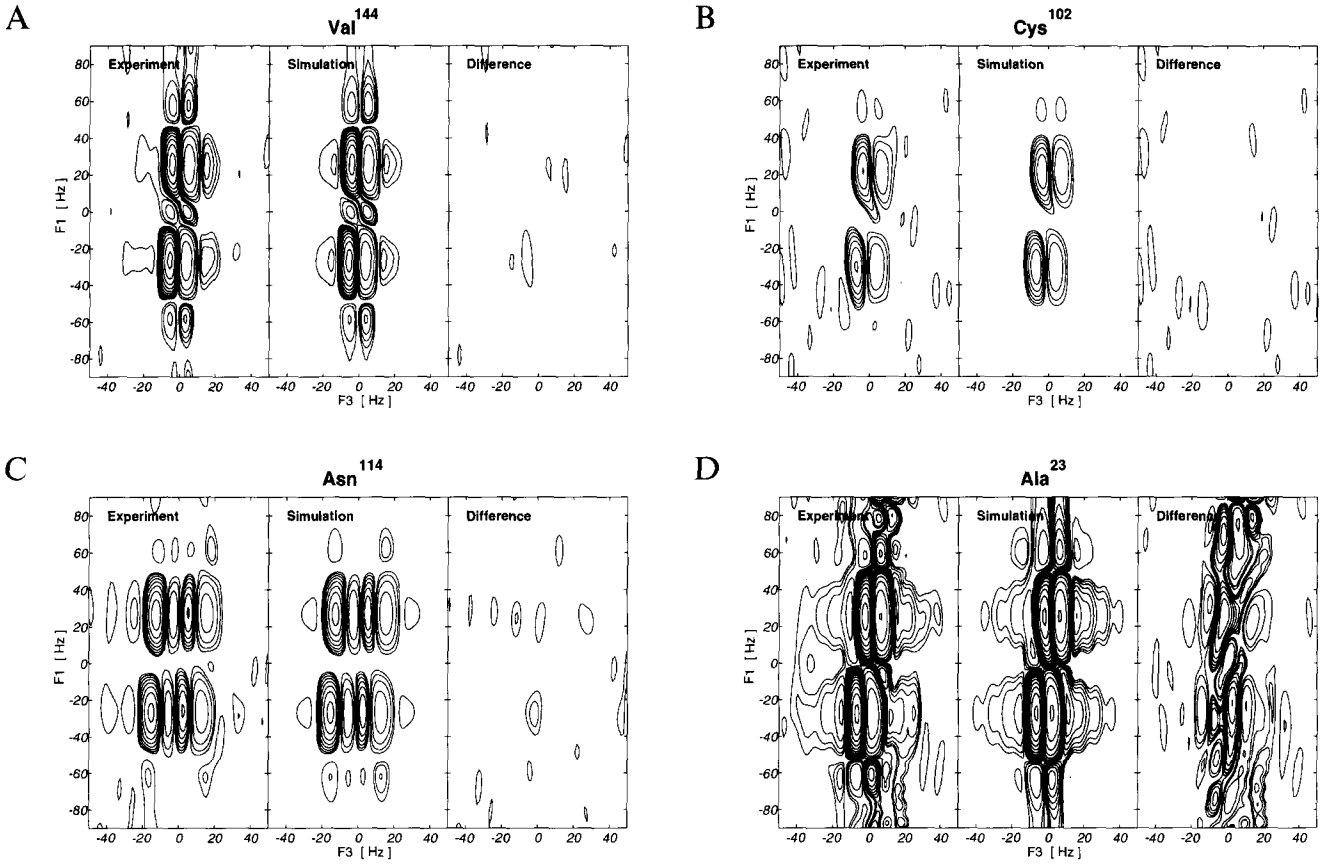

Fig. 3. Representative (ω_1,ω_3) projections of experimental C^α,H^N and C^α,H^β multiplets, obtained from a sample of ^{13}C-enriched *Desulfovibrio vulgaris* flavodoxin at 300 K using the heteronuclear relayed E.COSY pulse sequence depicted in Fig. 1. Positive and negative contours are drawn with level spacings of $\sqrt{2}$ and 2, respectively, with the lowest level at twice the rms noise intensity. Quantitative evaluation of the $^3J(H^N,C')$ and $^3J(H^N,C^\beta)$ coupling constants was achieved by iterative multiplet simulation, as described in the text. (A) The C^α,H^N multiplet of Val^{144} (ω_1 = 66.9 ppm, ω_3 = 8.05 ppm) represents a good fit (100% significance from ANOVA) for an intermediate $^3J(H^N,C')$ coupling constant typical of α-helix conformations. (B) Cys^{102} (63.4,9.73 ppm) participates in the FMN binding site: a large $^3J(H^N,C')$ coupling constant is recognized in the C^α,H^N multiplet. (C) The C^α,H^β multiplet of Asn^{114} (56.9,3.03 ppm) shows a large additional in-phase splitting along the acquisition dimension due to the geminal $^2J(H^{\beta2},H^{\beta3})$ coupling typical of residues containing two H^β protons in the side chain. (D) The robustness of the numerical evaluation procedure is demonstrated with the C^α,H^β multiplet of Ala^{23} (56.8,1.39 ppm), which is located on a t_1 noise ridge and is very hard to analyze with other methods. Although the fit is less significant (72% from ANOVA), multiplet simulation allows the $^3J(H^\beta,C')$ coupling constant to be determined with sufficient precision.

Spectrum acquisition and processing

The 3D (^{13}C,^1H,^1H)-heteronuclear relayed E.COSY experiment shown in Fig. 1 was carried out on a Bruker AMX-600 spectrometer equipped with a 5-mm triple-resonance probe. The experiment was conducted at 300 K. The proton rf carrier was set on the water resonance, which was saturated by low-power irradiation during the relaxation period. Nonselective proton π/2 pulses had a length of 10.8 μs, while band-selective ^{13}C excitation pulses employed 1.152-ms G4 and 378-μs G3 Gaussian cascades (Emsley and Bodenhausen, 1990) for π/2 and π pulses, respectively. The second G4 pulse had a time-reversed envelope. Band-selective ^{13}C decoupling during acquisition was achieved with G3-MLEV16 expansions (Eggenberger et al., 1992a) consisting of 512-μs G3 pulses. Using the GARP composite-pulse decoupling scheme (Shaka et al., 1985), ^{15}N nuclei were decoupled during all periods, except the relaxation delay. The carbon rf carrier was positioned at the center of the C^α chemical-shift range to apply G4 π/2 pulses. The G3 inversion pulse and the band-selective decoupling sequence were phase modulated such that the virtual carrier was 2 kHz upfield. The period τ for the evolution of $^1J(H^\alpha,C^\alpha)$ couplings was set to 3.4 ms. The constant time T was 27.0 ms in order to refocus $^1J(C^\alpha,C^\beta)$ couplings. The spectral widths covered 4808, 2404 and 9091 Hz in the ω_1, ω_2 and ω_3 dimensions, respectively. TPPI (Marion and Wüthrich, 1983) and States-TPPI (Marion et al., 1989) schemes were employed for quadrature detection in the ω_1 and ω_2 dimensions, respectively. The data set was recorded within 91 h, collecting 252 (real)×32 (complex)×2K (real) points. The acquisition times were 26.2, 13.3 and 112.7 ms in the t_1, t_2 and t_3 dimensions, respectively. Acquisition was triggered such that a 180° linear phase correction was required after Fourier transformation to achieve an optimally flat baseline in ω_3 (Marion and Bax, 1988).

The data matrix was Fourier transformed to 1K×64×2K real points to yield spectral resolutions of 4.70, 37.6

and 4.44 Hz in the ω_1, ω_2 and ω_3 dimensions, respectively. Prior to Fourier transformation, t_1 and t_2 data were extended to 336 real and 42 complex points using linear prediction. Squared-cosine, squared-sine shifted by $\pi/2.5$ rad, and sine functions were used for apodization in the t_1, t_2 and t_3 dimensions. The use of selective G4/G3 pulses with long duration required a linear phase correction in the ω_1 dimension. No phase correction was needed in the ω_2 dimension. Finally, pure absorptive parts of the C^α,H^N and C^α,H^β multiplets in the heteronuclear relayed E.COSY spectrum were displayed as two-dimensional (ω_1,ω_3)-projections calculated by summing over 1–3 appropriate ω_2 slices, as illustrated in Fig. 3.

Computer analysis of multiplet patterns

Experimental heteronuclear relayed E.COSY multiplets (M^{exp}) were handled as 2D matrices of 32×64 data points, each being centered at the approximate (ω_1,ω_3) chemical-shift coordinates of the selected signal. The simulated multiplet patterns (M^{sim}) were obtained by a 2D Fourier transformation of the (t_1,t_3) FID signals computed from the correspondingly reduced set of operator products given in Eq. 9, supplemented by relaxation and apodization effects. Relaxation was modeled by multiplying the t_3 time-domain signal with a decaying exponential function $r(t_3) = \exp(-\pi R t_3)$, where R is the apparent half-height line width in the ω_3 dimension. Relaxation effects were disregarded in computing t_1 signals, as the experiment was conducted in a constant-time fashion (Bax and Freeman, 1981; Rance et al., 1984). Apodization was accomplished by multiplying with filter functions identical to those used in spectrum processing, i.e., $h(t_1,t_3) = \cos^2(\pi t_1/2t_1^{max}) \sin(\pi t_3/t_3^{max})$. The initial line width was set to R = 10 Hz. The coupling parameters for C^α,H^N multiplets were initially 5, −1, 55 and 1 Hz for $^3J(H^N,H^\alpha)$, $^2J(C^\alpha,H^N)$, $^1J(C^\alpha,C')$ and $^3J(H^N,C')$, respectively; similar parameters were chosen in simulations of C^α,H^β multiplets. Two additional in-phase splitting parameters, related to t_1 and t_3, were found sufficient to account for the series of remote couplings indicated by the large product symbols in Eq. 9. These parameters were initially set to amino acid-specific values, e.g. 10 Hz and −15 Hz in the C^α,H^β multiplets assigned to residues bearing two geminal H^β protons. A zero-order phase parameter was implemented according to Eq. 8, in order to control the residual E.COSY multiplet phase distortion along ω_1 due to asymmetries from the collapsed ω_2 contributions. The position of the synthetic multiplet, i.e. the parameters Ω_{C^α} and Ω_{H^N} (or Ω_{H^β}), initially coincided with the center of gravity of the experimental multiplet and the rms intensity of the experimental multiplet was used for the initial amplitude.

A total of 11 parameters were considered in the optimization procedure (Table 1). The protocol included a repeatedly initialized optimization based on the BFGS quasi-Newton method (Broydon, 1970; Fletcher, 1970; Goldfarb, 1970; Shanno, 1970). Function gradients with respect to each of the parameters were provided to drive the mixed quadratic and cubic line search algorithm. Although the results were found to be insensitive to moderate variations in the initial parameter estimates, it turned out that in particular the use of function gradients was critical to avoid unrecoverable off-shoots in the initial stages. The convergence criterion was set to a fractional tolerance of 10^{-4} in the parameter and function values. Typically, 500 function and 150 gradient evaluations were needed for each multiplet simulation, requiring approximately 3 min of CPU time on a MIPS R4000-SC-based Silicon Graphics Indy workstation. The results for the three-bond coupling parameters of interest are summarized in Table 2.

Error and significance analysis

The agreement between simulated and experimental data was characterized in a least-squares sense by the normalized fit error $\varepsilon^2 = \varepsilon_{noise}^{-2} \Sigma_i^n (M_i^{exp} - M_i^{sim})^2$, where i runs over all n multiplet points and ε_{noise} is the rms noise amplitude obtained from empty regions in the spectrum. Given that uncorrelated random errors affect the spectrum points uniformly, the variance–covariance matrix of the final parameters $\mathbf{C} = \varepsilon_{noise}^2 (\mathbf{D}^\dagger \mathbf{D})^{-1}$ (Clifford, 1973), where $\mathbf{D}$ represents the matrix of partial derivatives $D_{ik} = \partial M_i / \partial P_k$ of the spectrum point M_i with respect to the parameter P_k. The derivatives were numerically evaluated using the gradient subroutine mentioned above. From the trace of the variance–covariance matrix $\mathbf{C}$, the statistical standard deviations in the final parameters, $\sigma_k = (C_{kk})^{1/2}$, were derived.

Statistical standard deviations significantly underestimate errors due to experimental misadjustments and to the intrinsic nonlinear properties of the model function. Therefore, confidence boundaries for the parameters were derived from the fractional increase in the sum of squares of residuals, computed according to:

$$\frac{\varepsilon_{max}^2}{\varepsilon_{min}^2} = 1 + \frac{p-1}{n-p} \cdot F(p-1, n-p, \alpha) \qquad (10)$$

where n and p are the number of observables (i.e., the number of multiplet data points) and fit parameters, respectively, and F is the Fisher variance ratio. For a given acceptance probability of $(1 - P) = 68.3\%$, i.e., for one standard deviation based on the assumption of a multivariate Gaussian distribution in parameter space, the critical value for a two-tailed test on the F-distribution inserted into Eq. 10 was $F(10, 2037, 0.841) = 1.435$ (Merrington and Thompson, 1948; Sokal and Rohlf, 1981). Thus, the bounding ε^2 variance ratio associated with the 2048 residuals and 11 parameters amounts to 1.0070.

TABLE 2
THREE-BOND J-COUPLING CONSTANTS (Hz) IN *DESULFOVIBRIO VULGARIS* FLAVODOXIN (OXIDIZED) DETERMINED FROM A 3D HETERONUCLEAR RELAYED E.COSY SPECTRUM[a]

Residue	ϕ-related	χ_1-related		Residue	ϕ-related	χ_1-related	
	$^3J(H^N,C')$	$^3J(H^{\beta x},C')$	$^3J(H^{\beta y},C')$		$^3J(H^N,C')$	$^3J(H^{\beta x},C')$	$^3J(H^{\beta y},C')$
Pro^2		3.21 ± 1.09	0.88 ± 1.12	Thr^{59}	0.06 ± 0.26		0.16 ± 0.62
Lys^3	0.18 ± 0.10		3.51 ± 0.65	Trp^{60}	1.56 ± 0.25	2.51 ± 0.50	1.19 ± 0.95
Ala^4	0.97 ± 0.15	4.00 ± 0.10		Asp^{62}	1.66 ± 0.43	2.83 ± 0.86	4.08 ± 0.63
Leu^5	0.67 ± 0.49 >>>			Asp^{63}	2.38 ± 0.82 >	3.37 ± 0.71	2.35 ± 0.61
Ile^6	1.15 ± 0.26 >	2.69 ± 0.86		Ser^{64}	2.66 ± 0.20		
Val^7	0.93 ± 0.15	2.48 ± 0.47		Ile^{65}	1.02 ± 0.18 >	2.92 ± 0.41	
Tyr^8	0.91 ± 0.10	–		Glu^{66}	2.07 ± 0.96 <		
Ser^{10}	1.79 ± 0.41			Leu^{67}	0.24 ± 0.44		
Thr^{11}	−0.59 ± 0.49			Gln^{68}	1.67 ± 1.15 <		
Thr^{12}	0.32 ± 0.44			Asp^{69}			2.65 ± 0.16
Asn^{14}				Asp^{70}	0.09 ± 0.39	1.96 ± 0.66	
Thr^{15}				Phe^{71}	0.07 ± 0.16	3.97 ± 0.62	
Glu^{16}	0.32 ± 0.51 <	1.80 ± 0.91		Ile^{72}	2.09 ± 0.61 <		1.46 ± 0.33
Tyr^{17}			1.82 ± 0.98	Pro^{73}		1.82 ± 0.72	4.32 ± 0.75
Thr^{18}	1.63 ± 0.61	1.58 ± 0.87		Leu^{74}	0.52 ± 0.15	2.32 ± 0.46	
Ala^{19}	1.61 ± 0.27			Phe^{75}	1.42 ± 0.59	2.22 ± 0.76	
Glu^{20}	1.66 ± 0.18	4.48 ± 0.55	3.80 ± 1.13	Asp^{76}	1.48 ± 0.20		–
Thr^{21}	1.17 ± 0.25	0.80 ± 0.37		Ser^{77}	0.35 ± 0.22		
Ile^{22}	1.31 ± 0.31 >	1.46 ± 0.49		Leu^{78}	3.24 ± 0.60	3.55 ± 0.41	4.69 ± 0.51
Ala^{23}	2.60 ± 0.88	4.36 ± 0.30		Glu^{79}	2.05 ± 0.37		
Arg^{24}	1.55 ± 0.42	2.46 ± 1.22	4.92 ± 1.01	Glu^{80}			0.10 ± 0.49
Glu^{25}				Thr^{81}	0.79 ± 0.11		
Leu^{26}	1.09 ± 0.32	1.08 ± 0.45		Ala^{83}	1.21 ± 0.15		4.05 ± 0.08
Ala^{27}	1.30 ± 0.58	4.42 ± 0.08		Gln^{84}			
Asp^{28}	1.47 ± 0.22 <	2.40 ± 0.29	3.62 ± 1.23	Arg^{86}	−0.12 ± 0.18	2.64 ± 0.94	
Ala^{29}	0.28 ± 0.11	4.22 ± 0.31		Lys^{87}	0.34 ± 0.57	2.23 ± 1.22	
Tyr^{31}	−0.15 ± 0.22	1.70 ± 0.97		Val^{88}	0.89 ± 0.09		2.67 ± 0.69
Glu^{32}	0.10 ± 0.23		2.26 ± 1.41	Ala^{89}	3.27 ± 0.32		4.20 ± 0.12
Val^{33}	0.31 ± 0.17	2.99 ± 0.80		Cys^{90}	−0.07 ± 0.21		–
Asp^{34}	0.94 ± 0.32 >>	2.56 ± 0.86		Phe^{91}	2.06 ± 0.12 >		
Ser^{35}	0.58 ± 0.10	3.65 ± 0.48	4.93 ± 0.78	Cys^{93}	0.12 ± 0.46 <<<		
Arg^{36}				Asp^{95}	1.94 ± 0.31 >>		–
Asp^{37}	0.21 ± 0.16	4.42 ± 0.78		Ser^{96}	1.05 ± 0.33 <		
Ala^{38}	2.53 ± 0.35			Ser^{97}	0.31 ± 0.08	4.43 ± 1.15	1.64 ± 0.42
Ala^{39}	1.53 ± 0.18	4.23 ± 0.51		Tyr^{98}	−0.06 ± 0.18 >		1.64 ± 1.02
Ser^{40}	0.13 ± 0.16	0.83 ± 0.93		Glu^{99}	2.04 ± 0.33	6.92 ± 0.80	1.96 ± 0.54
Val^{41}	0.30 ± 0.09			Tyr^{100}	1.28 ± 0.63 <<		
Glu^{42}	0.65 ± 0.10	3.66 ± 0.93		Phe^{101}			
Ala^{43}	1.63 ± 0.32			Cys^{102}	3.07 ± 0.39 <		0.15 ± 1.28
Leu^{46}			1.84 ± 0.43	Ala^{104}	0.67 ± 0.29		
Phe^{47}				Val^{105}	0.56 ± 0.21		1.88 ± 0.28
Glu^{48}	1.37 ± 0.40	–		Asp^{106}	1.94 ± 0.38		–
Phe^{50}	−0.17 ± 0.23		0.93 ± 1.42	Ala^{107}	1.57 ± 0.14		4.33 ± 0.28
Asp^{51}			1.24 ± 1.32	Ile^{108}	0.93 ± 0.24		1.79 ± 0.27
Leu^{52}		–		Glu^{109}	1.72 ± 0.47	1.91 ± 0.61	
Val^{53}	0.35 ± 0.57	2.22 ± 1.41		Glu^{110}	1.88 ± 0.37	4.79 ± 3.02	0.10 ± 1.59
Leu^{54}	0.60 ± 0.21	1.69 ± 0.88		Lys^{111}	0.94 ± 0.24		3.06 ± 0.74
Leu^{55}				Leu^{112}	1.43 ± 0.36	1.01 ± 0.63	
Cys^{57}	1.91 ± 0.37	5.21 ± 1.41		Lys^{113}	1.57 ± 0.20		–
Ser^{58}	0.10 ± 0.38			Asn^{114}	1.30 ± 0.35	2.70 ± 0.21	1.73 ± 1.08

[a] $H^{\beta x}$ and $H^{\beta y}$ designate low-field and high-field resonances, respectively, irrespective of the stereospecific assignments of H^β protons (see text). Side-chain couplings in residues bearing two H^β protons with degenerate chemical shifts within 0.05 ppm were not evaluated (–). The $^3J(H^\beta,C')$ coupling constants in threonine, valine and isoleucine residues are unique. Alanine $^3J(H^\beta,C')$ coupling constants represent conformationally averaged values due to methyl group rotation. Glycine entries in positions 9, 13, 30, 44, 45, 49, 56, 61, 82, 85, 92, 94, 103, 116, 123, 128, 139, and 146 are deliberately omitted, as the presence of two H^α protons complicates numerical multiplet analysis. For convenience, $^3J(H^N,C')$ coupling constants are compared to recent results (Löhr and Rüterjans, 1995) where the symbols '>' and '<' indicate the corresponding number of 0.5-Hz increments by which the present coupling constants differ from the previous ones towards larger and smaller values, respectively.

TABLE 2 (continued)

Residue	ϕ-related $^3J(H^N,C')$	χ_1-related $^3J(H^{\beta x},C')$	$^3J(H^{\beta y},C')$	Residue	ϕ-related $^3J(H^N,C')$	χ_1-related $^3J(H^{\beta x},C')$	$^3J(H^{\beta y},C')$
Leu[115]	0.40 ± 0.11	1.67 ± 0.68		Ala[133]	0.63 ± 0.14	3.96 ± 0.09	
Ala[117]	0.55 ± 0.34	4.41 ± 0.16		Arg[134]	3.61 ± 0.73		2.47 ± 0.55
Glu[118]	0.18 ± 0.11			Asp[135]	1.14 ± 0.22	–	
Ile[119]	0.56 ± 0.42	1.62 ± 0.71		Asp[136]	0.79 ± 0.34 >	−0.08 ± 0.67	
Val[120]	1.09 ± 0.08	1.58 ± 0.48		Ile[137]	1.05 ± 0.30	2.17 ± 0.45	
Gln[121]	3.04 ± 0.15	–		Val[138]	1.37 ± 0.29	1.27 ± 0.36	
Asp[122]	1.93 ± 0.56		2.43 ± 0.47	Trp[140]	1.68 ± 0.44 >	–	
Leu[124]	−0.24 ± 0.31 <<	2.57 ± 1.32		Ala[141]	1.57 ± 0.27	4.15 ± 0.54	
Arg[125]	1.06 ± 0.78 >			His[142]	1.16 ± 0.46		4.74 ± 0.84
Ile[126]	−0.58 ± 0.21	1.52 ± 0.54		Asp[143]	1.22 ± 0.23		
Asp[127]	0.46 ± 0.44	4.83 ± 1.53		Val[144]	1.39 ± 0.08	2.81 ± 0.24	
Asp[129]		2.57 ± 1.25		Arg[145]	1.74 ± 0.18	3.45 ± 2.02	
Pro[130]		–		Ala[147]	0.49 ± 0.06	4.12 ± 0.36	
Arg[131]			0.25 ± 1.27	Ile[148]	0.78 ± 0.03	1.77 ± 0.20	
Ala[132]		4.19 ± 0.59					

The deviations in each of the optimum parameters, required to increase the sum of squares of the residuals from ε^2_{min} to the threshold ε^2_{max}, were iteratively determined using a modified secant algorithm (Press et al., 1989). The asymmetry of the ε^2 isocontour on the error hypersurface was tested with a bidirectional search, using positive and negative deflections in each single parameter. The cross-correlation in the parameters was assessed by repeating the bidirectional ε^2 boundary search along the principal axes of the covariance Eigenbase (Johnson, 1983), i.e., by simultaneously changing all parameters with relative scales given by the statistical standard deviations σ_k computed before. The projection onto the parameter space was accomplished by the transformation $\mathbf{V} = \sigma \cdot \mathbf{X}^{-1}$, where $\mathbf{X}$ is the covariance eigenvector matrix and the matrix columns of $\mathbf{V}$ are the projection vectors denoting the search path associated with a particular principal axis. It was found that the asymmetry of the ε^2 isocontour was negligible for the desired three-bond coupling parameters, so that the confidence interval was taken from the largest parameter deviation obtained in either search procedure. The results of the error calculation are also given in Table 2.

Results

In the course of an extensive study of the vicinal coupling constants in *D. vulgaris* flavodoxin, a modified version of the basic heteronuclear relayed E.COSY experiment (Schmidt et al., 1995) has been employed. From a single 3D heteronuclear correlation spectrum, 109 C^α,H^N and 100 C^α,H^β two-dimensional multiplets were subjected to an iterative fitting procedure, aimed at the accurate determination of the $^3J(H^N,C')$ and $^3J(H^\beta,C')$ coupling constants. $^3J(H^N,C')$ couplings in glycine were not evaluated, as the presence of two large $^1J(H^\alpha,C^\alpha)$ couplings in these residues gives rise to a complicated C^α,H^N multiplet; in addition, the experimental condition $(T + 2\tau) \approx (2J_{H^\alpha H^\alpha})^{-1}$ with respect to the homonuclear geminal coupling makes the multiplet intensity vanish. Selected examples of the agreement between experiment and simulation are shown in Fig. 3. The coupling constants and their associated errors are listed in Table 2.

The magnitudes of the $^3J(H^N,C')$ coupling constants in *D. vulgaris* flavodoxin range from −0.6 Hz (Thr^{11}) up to +3.6 Hz (Arg^{134}). A correlation between the $^3J(H^N,C')$ coupling constants and the global fold of the polypeptide backbone of *D. vulgaris* flavodoxin, which has recently been derived from NOE distance information (Knauf et al., 1993), is not obvious from the graphical representation in Fig. 4. Indeed, such ambiguity was expected, as the angular dependence of the $^3J(H^N,C')$ coupling constant (Bystrov, 1976; Wang and Bax, 1995) predicts similar values, on the order of 1–2 Hz, for both α-helix and β-sheet secondary structure elements. The largest value for the $^3J(H^N,C')$ coupling constant is expected if the torsion $\phi \approx 0°$ and can be used to recognize unusual conformations in the protein backbone (Ludvigsen and Poulsen, 1992). The $^3J(H^N,C')$ coupling constant is rather sensitive to twists originating from deviations (±20°) from ideal dihedral angles in a parallel β-sheet ($\phi = -120°$). In flavodoxin, residues 3–9, 32–36, 52–58, 86–93 and 124–127 are involved in β-sheet structures, while residues 13–28, 69–76, 104–114 and 134–148 participate in α-helix conformations (Watt et al., 1991; Knauf et al., 1993). In conclusion, the experimental $^3J(H^N,C')$ coupling constants agree with the NMR solution structure based on NOE distance information (Knauf et al., 1993), as well as with the results of X-ray diffraction studies on the recombinant protein (Watt et al., 1991).

From the multiplet simulations, the associated passive $^1J(C^\alpha,C')$ coupling constants were simultaneously obtained with high precision. These couplings potentially provide

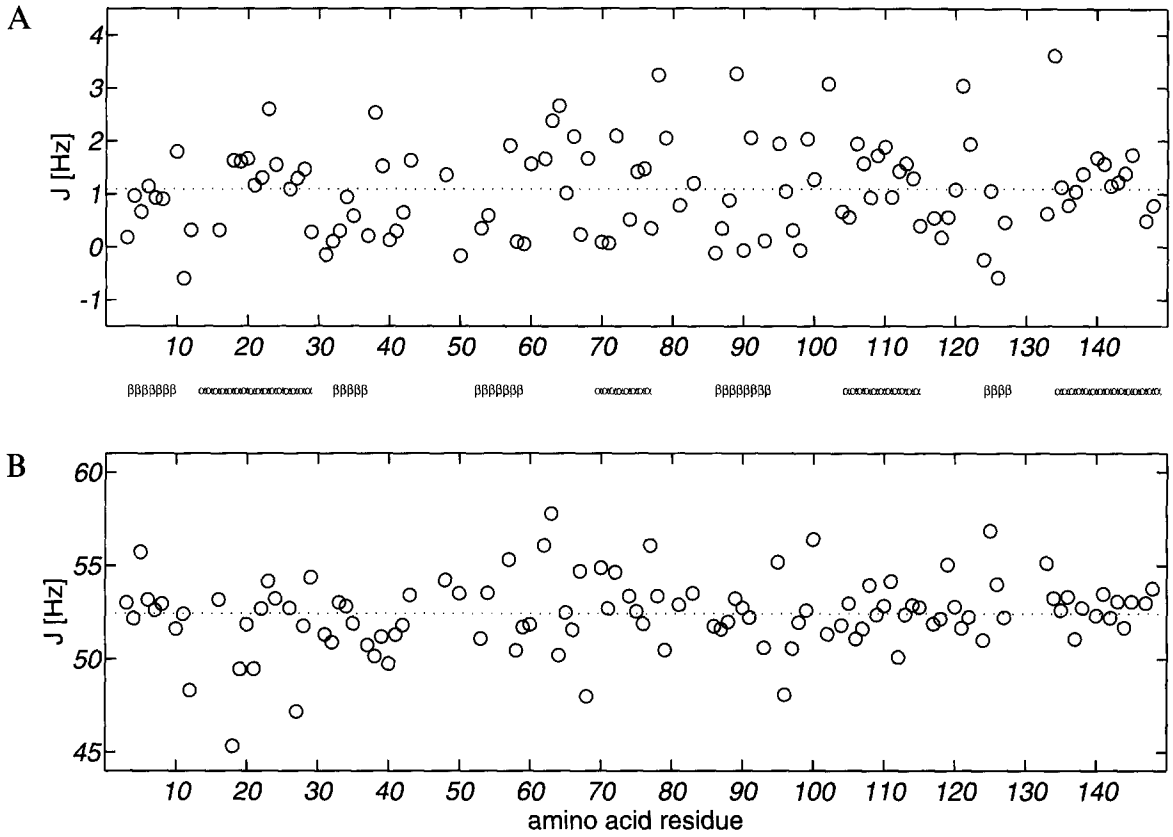

Fig. 4. Experimental J-coupling constants in *Desulfovibrio vulgaris* flavodoxin plotted against the residue sequence. (A) $^{3}J(H^{N},C')$ coupling constants; (B) $^{1}J(C^{\alpha},C')$ coupling constants. The dotted lines represent ensemble average values for the respective coupling constants. The magnitudes of the couplings show no correlation with α-helix and β-sheet secondary structure elements, indicated by symbols.

information about local variations in the bond angles of planar or tetrahedral sites. The use of one-bond couplings in structure analysis is not yet much developed and has been demonstrated only in a few cases, i.e., with heteronuclear $^{1}H,^{13}C$ interaction (Vuister et al., 1992,1993), with $^{1}H,^{15}N$ couplings (Beinert et al., 1985) and with $^{13}C,^{15}N$ couplings (Juranic et al., 1995). The distribution of the $^{1}J(C^{\alpha},C')$ coupling constants in flavodoxin exhibits a narrow range of 52.4 ± 1.9 Hz, averaged over the 109 values determined in C^{α},H^{N} multiplet simulations. However, no dependence on secondary structure is perceived from Fig. 4, and correlation with hydrogen-bonding patterns (Juranic et al., 1995) failed as well.

The $^{3}J(H^{\beta},C')$ coupling constants in *D. vulgaris* flavodoxin determined in the present work extend the known $^{3}J(H^{\beta},C')$ coupling constants determined by other NMR correlation techniques (Weisemann et al., 1994a). The dependence of the $^{3}J(H^{\beta},C')$ coupling constant on the dihedral angle conformation has been given by Fischman and co-workers (1980). From 13 out of the 17 alanine residues in flavodoxin, the mean $^{3}J(H^{\beta},C')$ coupling constant due to conformational averaging about the side-chain torsion χ_1 amounts to 4.20 ± 0.15 Hz. The $^{3}J(H^{\beta},C')$ coupling constants facilitate the stereospecific H^{β} resonance assignments of diastereotopic methylene proton positions in a joint analysis of $^{3}J(H^{\beta},H^{\alpha})$, $^{3}J(H^{\beta},C')$, and $^{3}J(H^{\beta},N)$ coupling constants. A quantitative evaluation of the backbone torsions ϕ and side-chain torsions χ_1 in *D. vulgaris* flavodoxin, based on the coupling constants determined, will be presented in a forthcoming paper.

Discussion and Conclusions

The proposed 3D heteronuclear relayed E.COSY pulse sequence is a comparably robust J-coupling correlation experiment and, importantly, the analytical description of the spin response is tractable. The fact that heteronuclear relayed E.COSY involves a minimal number of pulses renders this technique suitable for quantitative multiplet simulation, to tackle even such complicated spin topologies as encountered in ^{13}C-enriched polypeptides. The benefit of E.COSY-type correlation (Griesinger et al., 1986), compared to quantitative J-correlation (Bax et al., 1994), lies in the capability to determine vanishingly small couplings, which particularly applies to the measurement of usually small $^{3}J(H^{N},C')$ coupling constants in proteins.

The improvements of the proposed 3D experiment over the general 2D pulse scheme (Schmidt et al., 1995) are the following: (i) the extension to a third dimension reduces spectral overlap in applications to proteins; (ii) constant-time and decoupling schemes remove undesired multiplet splittings in ω_1 due to $^{1}J(C^{\alpha},C^{\beta})$ and $^{3}J(H^{N},H^{\alpha})$ or $^{3}J(H^{\alpha},$

H^{β}) as well as $^{1}J(H^{\beta},C^{\beta})$ in the acquisition dimension, in order to assist resolution of $^{1}J(C^{\alpha},C')$ splittings in the presence of broad lines; (iii) the use of selective excitation approximates the small-flip-angle limit, i.e. $\beta = 0°$, for perfect cancellation of undesired E.COSY contributions; and (iv) a specific coupling topology is picked by selective excitation, which minimizes experiment time due to reduced spectral widths.

The foundation of heteronuclear relayed E.COSY is the intermediate creation of heteronuclear multiple-quantum coherence (HMQC) during the evolution period(s). HMQC sequences lead to very efficient coherence transfer, as a variety of essential chemical shifts and couplings evolve simultaneously. Undesired multiplet J-splittings along the indirectly sampled dimension in HMQC spectra due to proton–proton interactions would be reduced in heteronuclear single-quantum coherence (HSQC) experiments (Bodenhausen and Ruben, 1980), which rely on the intermediate creation of ^{13}C antiphase magnetization. However, the sizeable number of polarization-transfer events like pulses, and the indispensable additional relayed coherence transfer period in HSQC-type schemes impede straightforward numerical computation of the multiplet structure.

In view of the relaxation properties of proteins in solution, it has been pointed out that HMQC-type experiments may be superior to HSQC schemes due to the fact that the spectral density function associated with molecular motion is sampled differently (Seip et al., 1992). Relaxation effects, which spoil the desired E.COSY multiplet structure (Harbison, 1993; Norwood, 1993; Norwood and Jones, 1993), are minimized in the present pulse sequence, the more so since HMQC-COSY mixing schemes belong to the shortest conceivable proton-detected heteronuclear correlation experiments. Sophisticated experimental techniques like frequency-selective decoupling and doubly tuned excitation might also give rise to partially corrupt E.COSY multiplet patterns, due to off-resonance perturbation of the passive spin, i.e., C' in the present example. As a consequence, the measured coupling constant would be too small due to the partial reappearance of suppressed complementary E.COSY patterns (Griesinger et al., 1986). The problems connected to frequency-selective decoupling, like line-broadening, frequency-shift, and coherence-quenching effects, have been addressed in a series of papers by McCoy and Mueller (1992a–c). These effects were considered negligible in the present J-coupling evaluation, as the chemical-shift difference between typical protein C^{α} and C' resonances is large compared to the used excitation band width (Eggenberger et al., 1992a).

It can be argued that coherence, if transferred exclusively via one-bond couplings, might increase experimental sensitivity (Eggenberger et al., 1992b; Seip et al., 1994; Weisemann et al., 1994a,b). Here, we follow the strategy of avoiding experimental perturbation, e.g. a large number of mixing pulses, wherever possible, thereby trading ultimate sensitivity for simplicity in experimentation. Note also that any measurement of ϕ-related three-bond coupling constants in a protein, both heteronuclear $^{3}J(H^{N},C')$ and $^{3}J(H^{\beta},C')$ as well as homonuclear $^{3}J(H^{N},H^{\alpha})$ coupling constants, exploiting one-bond connectivity, involves insensitive coherence transfer via the 'bottleneck' $^{1}J(N,C^{\alpha})$ coupling, which is as small as 11 Hz (Delaglio et al., 1991). With respect to transfer efficacy, this does not differ significantly from the properties of the three-bond $^{3}J(H^{N},H^{\alpha})$ coupling exploited in the present scheme.

The presently determined $^{3}J(H^{N},C')$ coupling constants in *D. vulgaris* flavodoxin can be compared with those determined recently by an (H)CANNH experiment (Löhr and Rüterjans, 1995). On average, the previous values are slightly smaller, by approximately 0.1 Hz with a distribution in the differences of ± 0.5 Hz, than those determined by multiplet simulation (Table 2). This was attributed to the fact that the two-dimensional E.COSY multiplet fine structure possesses centrosymmetric features, for which 1D trace projection (Griesinger et al., 1987) and alignment (Karimi-Nejad et al., 1994; Schmidt et al., 1995) methods generally do not account. Under these circumstances, J-coupling evaluation might lead to incorrect (usually too small) values, unless the constituent multiplet lines are well resolved. The alternative method of computing the centres of gravity for each of the two multiplet halves (Emerson and Montelione, 1992; Montelione et al., 1992), which are well separated by the large $^{1}J(C^{\alpha},C')$ coupling for the C^{α},H^{N} and C^{α},H^{β} multiplets (Fig. 3), suffers from similar neglects. Since spectra of proteins the size of flavodoxin exhibit broad lines, an iterative computer fitting, which fully accounts for C_2-symmetric multiplet shapes, was chosen for extracting accurate J-coupling constants and their associated errors.

The error margins for J-coupling constants emerging from the analysis of variances (ANOVA) in F-statistics appear more plausible compared to the standard deviations determined in other work (Griesinger et al., 1987; Karimi-Nejad et al., 1994; Schmidt et al., 1994). Although small standard deviations indicate a reliable superposition of observed and simulated data and a large experimental signal-to-noise ratio, they exclusively reflect the statistical random error. In ANOVA and F-statistics, systematic bias arising from experimental misadjustments or t_1 noise ridges in the spectrum is at least partially accounted for, although the major issue is the consideration of the parameter cross-correlation, intrinsic to the model function.

We have demonstrated the applicability of the formalized heteronuclear relayed E.COSY method in view of coupling-constant determination in medium-sized proteins. It was shown that multiplet simulation in conjunction with multivariate error analysis improves the reliability of both accuracy and precision of the extracted J-coupling parameters, compared to conventional proce-

dures of J-coupling evaluation. Last but not least, the development of NMR multiplet simulation techniques provides a basis for fully automated E.COSY spectrum analysis.

Acknowledgements

We would like to thank Dr. Yasmin Karimi-Nejad for many stimulating discussions. Dr. Martin Knauf kindly provided coordinates of a preliminary solution structure of flavodoxin. We are indebted to Prof. Stephen Mayhew (Department of Biochemistry, University College Dublin) for help in preparation and labeling of *D. vulgaris* flavodoxin. A grant from the Deutsche Forschungsgemeinschaft (Ru 145/11-1) is gratefully acknowledged.

References

Bax, A. and Freeman, R. (1981) *J. Magn. Reson.*, **44**, 542–561.

Bax, A., Vuister, G.W., Grzesiek, S., Delaglio, F., Wang, A.C., Tschudin, R. and Zhu, G. (1994) *Methods Enzymol.*, **239**, 79–105.

Beinert, W.-D., Rüterjans, H. and Müller, F. (1985) *Eur. J. Biochem.*, **152**, 573–579.

Biamonti, C., Rios, C.B., Lyons, B.A. and Montelione, G.T. (1994) *Adv. Biophys. Chem.*, **4**, 51–120.

Bodenhausen, G. and Ruben, D.J. (1980) *Chem. Phys. Lett.*, **69**, 185–189.

Broydon, C.G. (1970) *J. Inst. Math. Applic.*, **6**, 76–90.

Bystrov, V.F. (1976) *Prog. NMR Spectrosc.*, **10**, 41–81.

Case, D.A., Dyson, H.J. and Wright, P. (1994) *Methods Enzymol.*, **239**, 392–416.

Clifford, A.A. (1973) *Multivariate Error Analysis*, Applied Science Publishers Ltd., London.

Curley, G.P., Carr, M.C., Mayhew, S.G. and Voordouw, G. (1991) *Biochemistry*, **30**, 7718–7730.

Delaglio, F., Torchia, D.A. and Bax, A. (1991) *J. Biomol. NMR*, **1**, 439–446.

Dubourdieu, M. and Fox, J.L. (1977) *J. Biol. Chem.*, **252**, 1453–1459.

Eberstadt, M., Gemmecker, G., Mierke, D.M. and Kessler, H. (1995) *Angew. Chem.*, **107**, 1813–1838; *Angew. Chem., Int. Ed. Engl.*, **34**, 1671–1695.

Eggenberger, U., Schmidt, P., Sattler, M., Glaser, S.J. and Griesinger, C. (1992a) *J. Magn. Reson.*, **100**, 604–610.

Eggenberger, U., Karimi-Nejad, Y., Thüring, H., Rüterjans, H. and Griesinger, C. (1992b) *J. Biomol. NMR*, **2**, 583–590.

Emerson, S.D. and Montelione, G.T. (1992) *J. Magn. Reson.*, **99**, 413–420.

Emsley, L.R. and Bodenhausen, G. (1990) *Chem. Phys. Lett.*, **165**, 469–476.

Fischman, A.J., Live, D.H., Wyssbrod, H.R., Agosta, W.C. and Cowburn, D. (1980) *J. Am. Chem. Soc.*, **102**, 2533–2539.

Fletcher, R. (1970) *Comput. J.*, **13**, 317–322.

Ghisla, S. and Massey, V. (1989) *Eur. J. Biochem.*, **181**, 1–17.

Goldfarb, D. (1970) *Math. Comput.*, **24**, 23–26.

Griesinger, C., Sørensen, O.W. and Ernst, R.R. (1986) *J. Chem. Phys.*, **85**, 6837–6852.

Griesinger, C., Sørensen, O.W. and Ernst, R.R. (1987) *J. Magn. Reson.*, **75**, 474–492.

Harbison, G.J. (1993) *J. Am. Chem. Soc.*, **115**, 3026–3027.

Johnson, M.L. (1983) *Biophys. J.*, **44**, 101–106.

Juranic, N., Ilich, P.K. and Macura, S. (1995) *J. Am. Chem. Soc.*, **117**, 405–410.

Karimi-Nejad, Y., Schmidt, J.M., Rüterjans, H., Schwalbe, H. and Griesinger, C. (1994) *Biochemistry*, **33**, 5481–5492.

Karplus, M. (1959) *J. Chem. Phys.*, **30**, 11–15.

Karplus, M. (1963) *J. Am. Chem. Soc.*, **85**, 2870–2871.

Knauf, M.A., Löhr, F., Curley, G.P., O'Farrell, P., Mayhew, S.G., Müller, F. and Rüterjans, H. (1993) *Eur. J. Biochem.*, **213**, 167–184.

Knauf, M.A., Löhr, F., Blümel, M., Mayhew, S.G. and Rüterjans, H. (1996) *Eur. J. Biochem.*, in press.

Löhr, F. and Rüterjans, H. (1995) *J. Biomol. NMR*, **5**, 25–36.

Ludvigsen, S. and Poulsen, F. (1992) *J. Biomol. NMR*, **2**, 227–233.

Marion, D. and Wüthrich, K. (1983) *Biochem. Biophys. Res. Commun.*, **113**, 967–973.

Marion, D. and Bax, A. (1988) *J. Magn. Reson.*, **79**, 352–356.

Marion, D., Ikura, M., Tschudin, R. and Bax, A. (1989) *J. Magn. Reson.*, **85**, 393–399.

Mayhew, S.G. and Ludwig, M.L. (1975) In *The Enzymes*, Vol. 12, 3rd ed. (Ed., Boyer, P.D.), Academic Press, New York, NY, pp. 57–118.

Mayhew, S.G. and Tollin, G. (1992) In *Chemistry and Biochemistry of Flavoenzymes*, Vol. 3, 3rd ed. (Ed., Müller, F.), CRC Press, Boca Raton, FL, pp. 389–426.

McCoy, M. and Mueller, L. (1992a) *J. Am. Chem. Soc.*, **114**, 2108–2112.

McCoy, M. and Mueller, L. (1992b) *J. Magn. Reson.*, **98**, 674–679.

McCoy, M. and Mueller, L. (1992c) *J. Magn. Reson.*, **99**, 18–36.

Merrington, M. and Thompson, C.M. (1948) *Biometrika*, **33**, 73–88.

Montelione, G.T., Emerson, S.D. and Lyons, B.A. (1992) *Biopolymers*, **32**, 327–334.

Norwood, T.J. (1993) *J. Magn. Reson. Ser. A*, **101**, 109–112.

Norwood, T.J. and Jones, K. (1993) *J. Magn. Reson. Ser. A*, **104**, 106–110.

Press, W.H., Flannery, B.P., Teukolsky, S.A. and Vetterling, W.T. (1989) *Numerical Recipes*, Cambridge University Press, Cambridge.

Rance, M., Wagner, G., Sørensen, O.W., Wüthrich, K. and Ernst, R.R. (1984) *J. Magn. Reson.*, **59**, 250–261.

Schmidt, J.M., Sørensen, O.W. and Ernst, R.R. (1994) *J. Magn. Reson. Ser. A*, **109**, 80–89.

Schmidt, J.M., Ernst, R.R., Aimoto, S. and Kainosho, M. (1995) *J. Biomol. NMR*, **6**, 95–105.

Seip, S., Balbach, J. and Kessler, H. (1992) *J. Magn. Reson.*, **100**, 406–410.

Seip, S., Balbach, J. and Kessler, H. (1994) *J. Magn. Reson. Ser. B*, **104**, 172–179.

Shaka, A.J., Barker, P.B. and Freeman, R. (1985) *J. Magn. Reson.*, **64**, 547–552.

Shanno, D.F. (1970) *Math. Comput.*, **24**, 647–656.

Sokal, R.R. and Rohlf, F.J. (1981) *Biometry – Statistical Tables*, 2nd ed., Freeman, New York, NY.

Vuister, G.W., Delaglio, F. and Bax, A. (1992) *J. Am. Chem. Soc.*, **114**, 9674–9675.

Vuister, G.W., Delaglio, F. and Bax, A. (1993) *J. Biomol. NMR*, **3**, 67–80.

Wang, A.C. and Bax, A. (1995) *J. Am. Chem. Soc.*, **117**, 1810–1813.

Watt, W., Tulinsky, A., Swenson, R.P. and Watenpaugh, K.D. (1991) *J. Mol. Biol.*, **218**, 195–208.

Weisemann, R., Löhr, F. and Rüterjans, H. (1994a) *J. Biomol. NMR*, **4**, 587–593.

Weisemann, R., Rüterjans, H., Schwalbe, H., Schleucher, J., Bermel, W. and Griesinger, C. (1994b) *J. Biomol. NMR*, **4**, 231–240.

Wüthrich, K. (1986) *NMR of Proteins and Nucleic Acids*, Wiley, New York, NY.